Hindawi Publishing Corporation
Mathematical Problems in Engineering
Volume 2014, Article ID 859890, 10 pages
http://dx.doi.org/10.1155/2014/859890

Research Article

Signal Processing for Digital Beamforming FMCW SAR

Qin Xin,[1] Zhihong Jiang,[1] Pu Cheng,[1] and Mi He[2]

[1] *College of Electronic Science and Engineering, National University of Defense Technology, ChangSha, Hunan 410073, China*
[2] *School of Biomedical Engineering, Third Military Medical University, Chongqing 400038, China*

Correspondence should be addressed to Pu Cheng; hagooddemon@163.com and Mi He; hmcherry@126.com

Received 10 November 2013; Revised 3 March 2014; Accepted 17 March 2014; Published 15 April 2014

Academic Editor: Gianluca Ranzi

According to the limitations of single channel Frequency Modulation Continuous Wave (FMCW) Synthetic Aperture Radar (SAR), Digital Beamforming (DBF) technology is introduced to improve system performance. Combined with multiple receive apertures, DBF FMCW SAR can obtain high resolution in low pulse repetition frequency, which can increase the processing gain and decrease the sampling frequency. The received signal model of DBF FMCW SAR is derived. The continuous antenna motion which is the main characteristic of FMCW SAR received signal is taken into account in the whole signal processing. The detailed imaging diagram of DBF FMCW SAR is given. A reference system is also demonstrated in the paper by comparing with a single channel FMCW SAR. The validity of the presented diagram is demonstrated with a point target simulation results.

1. Introduction

The combination of Frequency Modulated Continuous Wave (FMCW) technology and Synthetic Aperture Radar (SAR) paves a way to light-weight, cost-effective, high-resolution active microwave remote sensing instrument. This system is suitable for small platforms such as Unmanned Aerial Vehicles (UAV). In the last years, several FMCW SAR systems have been constructed and have been successfully used in ice measurement [1], environment monitoring [2], three-dimensional application [3], and so on [4, 5].

However, these systems are currently applied in the short range and narrow swath case. According to the single channel FMCW SAR radar equation [6], the most immediate method for improving the system performance is to increase the transmission power. Nevertheless, high power transmission is not a suitable solution because of the isolation problem between transmitter and receiver and the increasing system complexity. Moreover, when operating in high resolution such as 0.1 m mode, the aperture length of antenna in azimuth is very small. This will decrease the antenna gain of single channel FMCW SAR systems, and then it will decrease the Signal Noise Radio (SNR) of SAR images.

In pulsed SAR systems, wide unambiguous swath coverage and high azimuth resolution are also contradicting requirements. Several proposals, such as multiple beam SAR system operating in a squinted imaging geometry [7], displaced phase center antenna technique [8], quad array system [9], and High-Resolution Wide-Swath (HRWS) SAR system [10], have been presented to resolve the aforementioned dilemma. Those systems have their own advantages and disadvantages. However, their basic principle is ambiguity suppression using Digital Beamforming (DBF) technology combined with multiple antennas.

The HRWS SAR concept relies on separated transmit and receive antennas, which is also the characteristic of FMCW SAR systems. So the HRWS concept may be a suitable solution for improving the system performance of FMCW SAR. Now, multichannel FMCW SAR is becoming a hot area of miniature SAR research. And many research institutions have announced their research projects on multichannel FMCW SAR [11–14].

According to the imaging algorithm of pulsed DBF SAR, the basic steps are firstly the azimuth reconstruction and then single channel imaging. However, the multichannel azimuth reconstruction algorithm [15] is based on "stop and go"

hypothesis. Compared with pulsed SAR received signal, the main characteristic of FMCW SAR received signal is that the continuous antenna motion must be taken into account; that is, the "stop and go" hypothesis is not valid for FMCW SAR [16]. So the impact of continuous antenna motion to azimuth reconstruction must be analyzed. Furthermore, there are many imaging algorithms for single channel FMCW SAR. The best algorithm for DBF FMCW SAR when considering some nonideal factors such as sweep frequency nonlinearity should also be chosen carefully.

The remaining sections are organized as follows. Compared with single channel FMCW SAR, the performance improvement of DBF FMCW SAR is given in Section 2. The signal model, the impact of continuous antenna motion, and the complete imaging diagram of DBF FMCW SAR are all presented in Section 3. Next, an example system is designed and the numerical simulation results are given in Section 4. Finally, Section 5 concludes the whole paper.

2. Performance Improvement

The noise equivalent sigma zero (NESZ) is a quantity directly related to SAR imaging performance, which is defined as the target Radar Cross Section (RCS) when the SNR of the image is equal to one [17]. The NESZ of single channel FMCW SAR is expressed by [6]

$$\mathrm{NESZ} = \frac{(4\pi)^3 r^4 \sin\phi K T_0 F B_N L_s}{P_t G^2 \lambda^2 \rho_a \rho_r G_a G_r}, \tag{1}$$

where r is the slant range, ϕ is the incidence angle, K is the Boltzmann constant, T_0 is the system noise temperature, F is the receiver noise figure, B_N is the noise bandwidth, L_s is the loss factor, P_t is the transmitted signal power, G is the antenna gain, ρ_a and ρ_r are the azimuth and range resolution, respectively, and G_a and G_r are the azimuth and range processing gain, respectively.

2.1. Antenna Gain. From (1), we know that the transmit and receive antenna gains in single channel FMCW SAR system are the same. However, in DBF FMCW SAR, the receive antenna gain is not equal to that of the transmit antenna. Assum that MN receive channels are used, M is the antenna number in azimuth, and N is the antenna number in elevation. The multiple receive apertures are shown in Figure 1.

The DBF in azimuth is applied to suppress the azimuth ambiguity. This does not increase the antenna gain. In elevation, the channels are coherently combined. Performed by the SCan-On-REceive (SCORE) technique, the DBF in elevation can obtain full array gain over a wide area. Thus, under the same resolution and swath width, the maximum receive antenna gain of the DBF system is

$$G_{\mathrm{re}} = NG. \tag{2}$$

The DBF technique increases the antenna gain by N times, compared to the single channel system.

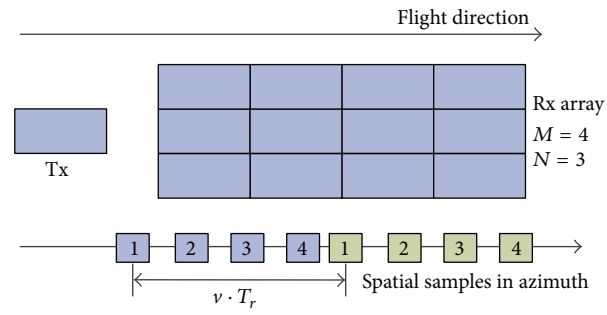

Figure 1: Illustration of multiple receive apertures.

2.2. Range Processing Gain. Range processing of FMCW SAR is analog with pulsed SAR. They are all based on pulse compressing using matched filter. Theoretically, range processing gain is about the following:

$$G_r = T_r B_r, \tag{3}$$

where T_r is the pulse width and B_r is the signal bandwidth. For FMCW SAR, the value of T_r is equal to $1/f_p$, where f_p is the pulse repetition frequency (PRF). If we decrease the system PRF using M receive channels in azimuth, we can get M times signal processing gain compared with single channel system. The signal processing gain is increased at the cost of long processing time.

2.3. Sampling Frequency. In order to maintain the low-power and lightweight characteristics of FMCW SAR, the sampling frequency should be chosen as lowly as possible. According to the Nyquist theorem, the lowest sampling frequency for FMCW SAR is

$$f_s = k_r \cdot \frac{2\left(r_{\max} - r_{\min}\right)}{c_0} = B_r f_p \cdot \frac{2\left(r_{\max} - r_{\min}\right)}{c_0}, \tag{4}$$

where k_r is the chirp modulation rate and $r_{\max}$ and $r_{\min}$ are the maximum and minimum slant range, respectively. The sampling frequency is also directly proportional to the PRF. That is to say, the sampling frequency of multichannel FMCW SAR is $1/M$ times of that of single channel FMCW SAR.

The DBF FMCW SAR operates with a low PRF to increase the swath width. To decrease the PRF, the significant and challenging processing is the azimuth ambiguity suppression. In the next section, we focus on the multichannel signal reconstruction in azimuth.

3. Signal Processing

3.1. Received Signal Model. Let the transmitted signal of FMCW SAR be written in complex form as follows:

$$ss_T(n,t) = \exp\left[j2\pi\left(f_c \cdot t + \frac{1}{2}k_r \cdot \left(t - nT_r\right)^2\right)\right], \tag{5}$$

where f_c is the center frequency, n is the sweep number, and t is the time variable. Because signal amplitude has little effect in SAR signal processing, so for simplicity, antenna

gain, amplitude effects of propagation on the signal and any additional time delays due to atmospheric effects are ignored in the following discussions.

The received signal is a delayed version of the transmitted one. The M channels of received signals in azimuth are processed. The mth received signal is

$$\begin{aligned} &ss_{m,R}(n,t) \\ &= \exp\left[j2\pi \left(f_c \cdot \left(t - \frac{r_{t,m}}{c_0} \right) + \frac{1}{2} k_r \right.\right. \\ &\qquad \left.\left. \cdot \left(t - nT_r - \frac{r_{t,m}}{c_0} \right)^2 \right) \right], \end{aligned} \tag{6}$$

where c_0 is the velocity of light and $r_{t,m}$ is the roundtrip instantaneous slant range which can be written as

$$r_{t,m}(t; r_0) = r_{tx}(t; r_0) + r_{rx,m}(t; r_0), \tag{7}$$

where $r_{tx}(t; r_0)$ and $r_{rx,m}(t; r_0)$ are transmit range and receive range, respectively. In the single channel case, $r_{tx}(t; r_0)$ is equal to $r_{rx,m}(t; r_0)$. However, it cannot be valid in the multichannel case. This is the main difference between the multichannel and the single channel FMCW SAR received signal.

Dechirp on receive is often used in FMCW SAR. In order to further decrease the sampling frequency, and then to decrease the data in range dimension, the radar demodulates the received signal by mixing it with a replica of the transmitted waveform delayed by a time $\tau_{\text{ref}} = 2 \cdot r_c / c_0$, where r_c is the slant range distance of the swath center. The reference signal is

$$\begin{aligned} &ss_{\text{ref}}(n,t; r_c) \\ &= \exp\left[j2\pi \left(f_c \cdot (t - \tau_{\text{ref}}) + \frac{1}{2} k_r \cdot (t - nT_r - \tau_{\text{ref}})^2 \right) \right]. \end{aligned} \tag{8}$$

The intermediate frequency signal that results from mixing (8) with (6) is

$$\begin{aligned} &ss_m(n,t; r_0) \\ &= \exp\left(-j \frac{2\pi f_c}{c_0} \cdot r_{t,m} \right) \cdot \exp\left[j \frac{\pi k_r}{c_0^2} \cdot (r_{t,m} - 2r_c)^2 \right] \\ &\quad \cdot \exp\left[-j \frac{2\pi k_r}{c_0} \cdot (r_{t,m} - 2r_c) \cdot \left(t - nT_r - \frac{2r_c}{c_0} \right) \right]. \end{aligned} \tag{9}$$

Using Taylor series, the round-trip range $r_{t,m}(t; r_0)$ can be expanded as

$$\begin{aligned} r_{t,m}(t; r_0) &= \sqrt{r_0^2 + v^2 t^2} + \sqrt{r_0^2 + (vt - \Delta x_m)^2} \\ &\approx \sqrt{r_0^2 + v^2 \cdot t_a^2} + \sqrt{r_0^2 + (vt_a - \Delta x_m)^2} - \lambda f_d t_r \\ &\approx 2r_0 + \frac{\Delta x_m^2}{4r_0} + \frac{(vt_a - \Delta x_m/2)^2}{r_0} - \lambda f_d t_r, \end{aligned} \tag{10}$$

where $t_a = nT_r$ and $t_r = t - nT_r$ represent azimuth time and range time, respectively. v is the velocity of the platform, r_0 is the closest distance between antenna and the scatter. Δx_m is the distance between the transmit antenna and the mth receive antenna, $\lambda = c_0 / f_c$ is the wavelength, and f_d is the approximate Doppler frequency shift during the transmission of one sweep as follows:

$$f_d = -\frac{1}{\lambda} \left[\frac{v^2 t_a}{\sqrt{r_0^2 + v^2 \cdot t_a^2}} + \frac{v(vt_a - \Delta x_m)}{\sqrt{r_0^2 + (vt_a - \Delta x_m)^2}} \right]. \tag{11}$$

Different from pulsed SAR, f_d introduced by the continuous antenna motion should be taken into consideration, for the "stop and go" hypothesis is not valid for FMCW SAR. This can be seen from the simulated results in Figure 5.

After substituting (10) into (9), the received signal of channel m can be rewritten as

$$\begin{aligned} &ss_m(t_a, t_r; r_0) \\ &= \exp\left(-j \frac{4\pi}{\lambda} \cdot r_0 \right) \cdot \exp\left[-j \frac{2\pi}{\lambda} \cdot \frac{\Delta x_m^2}{4r_0} \right] \\ &\quad \cdot \exp\left[-j \frac{2\pi}{\lambda} \cdot \frac{(vt_a - \Delta x_m/2)^2}{r_0} \right] \cdot \exp\left(j2\pi f_d t_r \right) \\ &\quad \cdot \exp\left[-j \frac{4\pi k_r}{c_0} \cdot (r(t_a; r_0) - r_c) \cdot \left(t_r - \frac{2r_c}{c_0} \right) \right] \\ &\quad \cdot \exp\left[j \frac{4\pi k_r}{c_0^2} \cdot (r(t_a; r_0) - r_c)^2 \right], \end{aligned} \tag{12}$$

where $r(t_a; r_0)$ is the azimuth dependent distance to the scatter which can be expressed by

$$r(t_a; r_0) \approx \sqrt{r_0^2 + v^2 \cdot t_a^2}. \tag{13}$$

In (12), the first to third exponential terms are the azimuth phase history of multichannel FMCW SAR. The fourth term represents the range cell migration due to continuous antenna motion, that is, the Doppler impact in one sweep. The fifth term represents the range signal, which is a sinusoidal signal with a constant frequency value corresponding to the azimuth dependent distance to the point target. The sixth exponential term represents the residual video phase (RVP) term.

3.2. The Impact of Continuous Antenna Motion. As mentioned above, the main characteristic of FMCW SAR is the continuous antenna motion. The range cell migration (RCM) introduced by the continuous antenna motion may result in reconstruction mismatch. Even worse, the extraphase term introduced by the continuous antenna motion may degrade the quality of the focus image.

Multichannel azimuth reconstruction algorithm [15] is a suited approach to process pulsed DBF SAR data in azimuth.

According to the algorithm [15] and the received signal model of DBF FMCW SAR described as (12), the reconstruction filters $\mathbf{P}(f_a)$ for DBF FMCW SAR can be calculated by the following equation:

$$\mathbf{P}(f_a) = \mathbf{H}^{-1}(f_a) = \begin{bmatrix} P_{11}(f_a) & P_{12}(f_a + f_p) & \cdots & P_{1M}(f_a + (M-1) f_p) \\ P_{21}(f_a) & P_{22}(f_a + f_p) & \cdots & P_{2M}(f_a + (M-1) f_p) \\ \vdots & \vdots & \vdots & \vdots \\ P_{M1}(f_a) & P_{M2}(f_a + f_p) & \cdots & P_{MM}(f_a + (M-1) f_p) \end{bmatrix}, \tag{14}$$

where $\mathbf{H}(f_a)$ is

$$\mathbf{H}(f_a) = \begin{bmatrix} \exp\left(-j\frac{\pi\Delta x_1^2}{2\lambda r_0}\right)\exp\left(-j\frac{\pi\Delta x_1}{v} f_a\right) & \cdots & \exp\left(-j\frac{\pi\Delta x_M^2}{2\lambda r_0}\right)\exp\left(-j\frac{\pi\Delta x_M}{v} f_a\right) \\ \exp\left(-j\frac{\pi\Delta x_1^2}{2\lambda r_0}\right)\exp\left(-j\frac{\pi\Delta x_1}{v}(f_a + f_p)\right) & \cdots & \exp\left(-j\frac{\pi\Delta x_M^2}{2\lambda r_0}\right)\exp\left(-j\frac{\pi\Delta x_M}{v}(f_a + f_p)\right) \\ \vdots & \vdots & \vdots \\ \exp\left(-j\frac{\pi\Delta x_1^2}{2\lambda r_0}\right)\exp\left(-j\frac{\pi\Delta x_1}{v}(f_a + (M-1) f_p)\right) & \cdots & \exp\left(-j\frac{\pi\Delta x_M^2}{2\lambda r_0}\right)\exp\left(-j\frac{\pi\Delta x_M}{v}(f_a + (M-1) f_p)\right) \end{bmatrix}. \tag{15}$$

Using basic matrix theory, the system matrix $\mathbf{H}$ can be decomposed as a matrix $\mathbf{Q}$ multiplied by a diagonal matrix $\mathbf{D}$, where only the elements of $\mathbf{D}$ are dependent on the slant range r_0. And the diagonal elements of $\mathbf{D}$ can be written as

$$(\mathbf{D})_{m,m} = \exp\left[-j\pi\frac{\Delta x_m^2}{2\lambda r_0}\right]. \tag{16}$$

In the SAR case, the range history is not a line but spans several range cells, which results in mismatch between the signal and the reconstruction. In FMCW SAR, the additional mismatch introduced by the continuous antenna motion is

$$\Delta\varphi_m = \frac{\pi\Delta x_m^2}{2\lambda} \cdot \frac{\Delta r_{\mathrm{dfm}}}{r_0 \cdot (r_0 + \Delta r_{\mathrm{dfm}})}, \tag{17}$$

in which Δr_{dfm} represents the maximum RCM introduced by the continuous antenna motion of channel m. The mismatch can be derived from (14) to (16).

Figure 2 shows a simulated RCM introduced by the continuous antenna motion using the parameter listed in Table 1. In this case, Δr_{dfm} is about 1 m. Calculated by (17), the mismatch introduced by this RCM is about 4×10^{-5} rad, which is negligible. Here, $\Delta x_m = 5$ m is assumed. On the other side, Δr_{dfm} is about 10 times of the range resolution. This RCM must be compensated according to SAR imaging theory [17]. In a word, for DBF FMCW SAR, the impact of continuous motion antenna is negligible during multichannel azimuth reconstructing [15]; however, it must be considered during RCM correction.

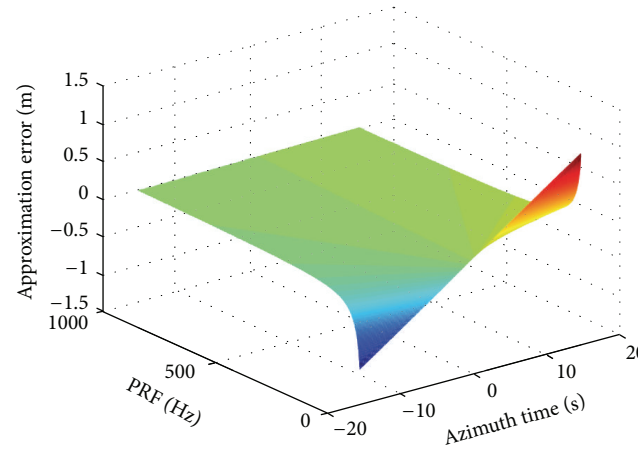

Figure 2: RCM introduced by the continuous antenna motion.

3.3. Signal Processing Diagram. The first part of signal processing for DBF FMCW SAR is the azimuth ambiguity suppression. All the recorded subaperture signals whose azimuth frequencies are aliasing become an equivalent single channel signal without azimuth ambiguity. To focus the signal, the second part of the diagram is the classic single channel SAR imaging.

In the first part, multichannel azimuth reconstruction algorithm [15] is chosen because the algorithm can relax the imposed constraints on system design and the algorithm performance is rarely affected by the continuous antenna

Table 1: System parameters.

Parameter	Multi-Channel System	Single Channel System
RF center frequency	15 GHz	15 GHz
Band Width	1.5 GHz	1.5 GHz
Operational Altitude	5000 m	5000 m
Operational Velocity	70 m/s	70 m/s
Swath Width	7 km	7 km
Resolution	0.1 m × 0.1 m	0.1 m × 0.1 m
Radar Losses	2 dB	2 dB
Incidence Angle	5–70°	5–70°
Number of Receive Apertures	2	1
Transmitted Power	5 W	5 W
Transmit Antenna Gain	19.5 dB	19.5 dB
Receive Antenna Gain	19.5 dB	19.5 dB
PRF	350 Hz	700 Hz
Range Processing Gain	66.3 dB	63.3 dB
Sampling Frequency	16 MHz	32 MHz

motion. In the second part, frequency scaling algorithm [16, 18–20] is combined with the DBF technology. This algorithm has not only efficient and accurate processing but also real-time integrated motion compensation [19] and easy sweep frequency nonlinear correction [16, 20].

The entire signal processing block diagram of DBF FMCW SAR is shown in Figure 3 including the following steps.

Step 1. Apply Azimuth Fast Fourier Transform (FFT) to the received signal of each channel. Then, the Doppler domain signal $Ss_m(f_a, t_r; r_0)$ is obtained, where f_a is the azimuth frequency.

Step 2. Design the azimuth reconstruction filter $\mathbf{P}(f_a)$ by using (14) and (15). The reconstruction filter of channel m can be written as

$$P_m(f_a) = \left[P_{m1}(f_a) \;\; P_{m2}(f_a) \;\; \cdots \;\; P_{mM}(f_a)\right]. \tag{18}$$

Step 3. Multiply each channel signal to the corresponding reconstruction filter. At this time, the signal becomes

$$Ss_{\mathrm{AR},m}(f_a, t_r; r_0) = Ss_m(f_a, t_r; r_0) \cdot P_m(f_a). \tag{19}$$

Step 4. Add each channel signal after passing the corresponding reconstruction filter. Then, we can obtain the equivalent single channel signal $Ss(f_a, t_r; r_0)$, which has nonazimuth frequency aliasing. And it can be written in convolution [16] as follows:

$$\begin{aligned} Ss(f_a, t_r; r_0) &= \left\{\exp\left(-j\frac{4\pi r_0\beta}{\lambda}\right)\exp(j2\pi f_d t_r)\right. \\ &\quad \cdot \exp\left[-j\frac{4\pi k_r}{c_0}\left(\frac{r_0}{\beta} - r_c\right)\left(t_r - \frac{2r_c}{c_0}\right)\right] \\ &\quad \left.\times \mathrm{src}(f_a, t_r; r_0)\right\} \\ &\quad \otimes \exp\left(-j\pi k_r t_r^2\right), \end{aligned} \tag{20}$$

where β is the RCM factor defined by

$$\beta(f_a) = \sqrt{1 - \frac{f_a^2\lambda^2}{4v^2}}, \tag{21}$$

where $\mathrm{src}(f_a, t_r; r_0)$ is the secondary range compression as follows:

$$\begin{aligned} \mathrm{src}(f_a, t_r; r_0) &= \exp\left[-j\frac{2\pi r_0 k_r^2\lambda}{c_0^2}\frac{\left(\beta^2 - 1\right)}{\beta^3}\left(t_r - \frac{2r_c}{c_0}\right)^2\right] \\ &\quad \cdot \exp\left[j\frac{2\pi r_0 k_r^3\lambda^2}{c_0^3}\frac{\left(\beta^2 - 1\right)}{\beta^5}\left(t_r - \frac{2r_c}{c_0}\right)^3\right]. \end{aligned} \tag{22}$$

Step 5 (frequency scaling transform). Multiplying the signal $Ss(f_a, t_r; r_0)$ with the frequency scaling factor, we have the following:

$$H_{\mathrm{FS}}(f_a, t_r) = \exp\left[j\pi k_r(1 - \beta)t_r^2\right]. \tag{23}$$

Step 6 (continuous antenna motion correction). Multiplying the signal with the Doppler frequency correction factor, we have the following:

$$H_{\mathrm{DFC}}(f_a, t_r) = \exp(-j2\pi f_d\beta \cdot t_r). \tag{24}$$

In actual implementation, Steps 5 and 6 can be completed at the same time. The signal $Ss_{\mathrm{FS}}(f_a, t_r; r_0)$ is obtained as follows:

$$Ss_{\mathrm{FS}}(f_a, t_r; r_0) = Ss(f_a, t_r; r_0) \cdot H_{\mathrm{FS}} \cdot H_{\mathrm{DFS}}. \tag{25}$$

After an equivalent transform, (25) can be expressed as

$$\begin{aligned} Ss_{\mathrm{FS}}(f_a, t_r; r_0) &= \left\{\exp\left(-j\frac{4\pi r_0\beta}{\lambda}\right)\right. \\ &\quad \times \exp\left[-j\frac{4\pi k_r}{c_0}\left(\frac{r_0}{\beta} - r_c\right)\left(\beta t_r - \frac{2r_c}{c_0}\right)\right] \\ &\quad \cdot \exp\left[-j\pi k_r\beta(\beta - 1)t_r^2\right] \\ &\quad \left.\times \mathrm{src}(f_a, \beta t_r; r_0)\right\} \otimes \exp\left(-j\pi k_r\beta t_r^2\right). \end{aligned} \tag{26}$$

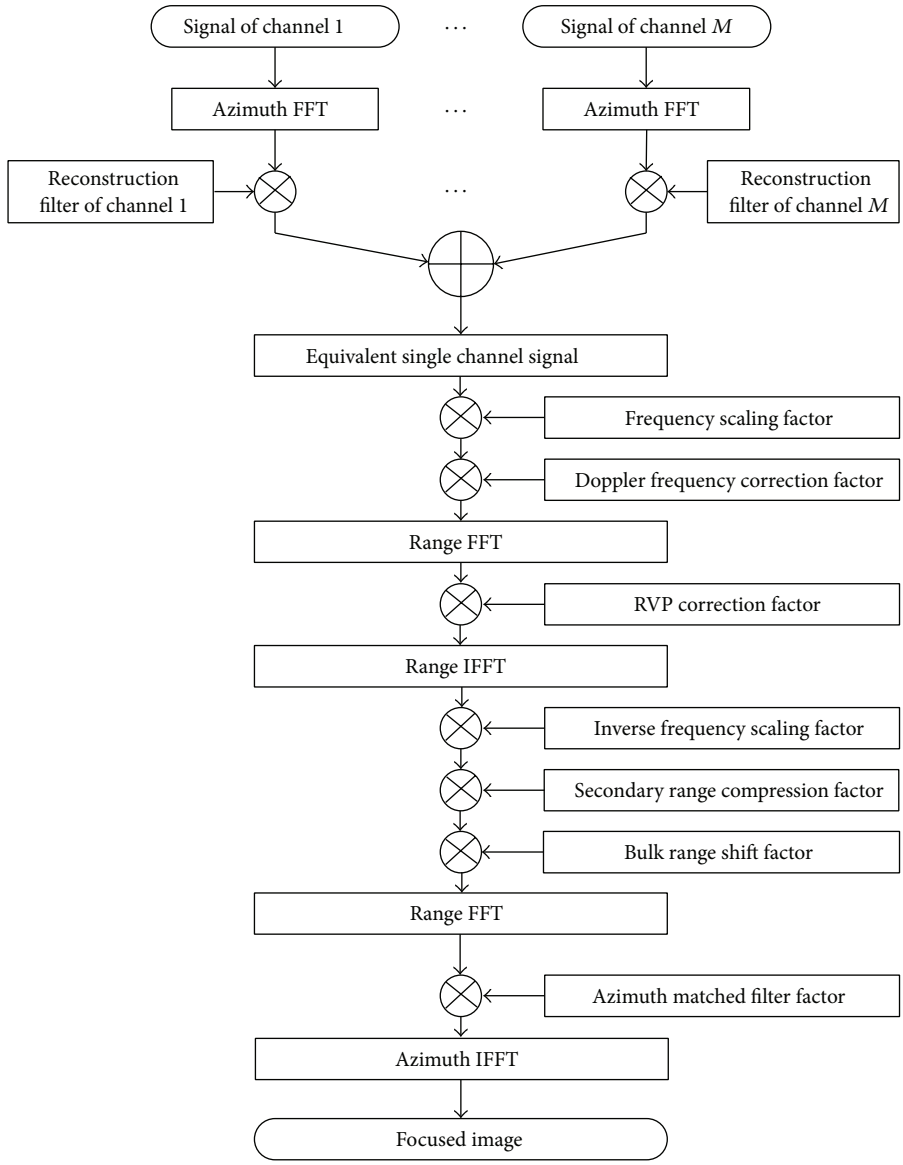

Figure 3: Signal processing block diagram for DBF FMCW SAR.

Step 7 (RVP correction). The correction is applied in 2D frequency domain. It is to eliminate the last exponential term in (26). After FFT in range dimension and multiplying with the RVP correction factor $H_{\mathrm{RVPC}}(f_a, f_r)$, IFFT in range domain is performed. The signal $Ss_{\mathrm{RVPC}}(f_a, t_r; r_0)$ is obtained as follows:

$$Ss_{\mathrm{RVPC}}(f_a, t_r; r_0) = \exp\left(-j\frac{4\pi r_0 \beta}{\lambda}\right) \exp\left[-j\frac{4\pi k_r}{c_0}\left(\frac{r_0}{\beta} - r_c\right)\left(\beta t_r - \frac{2r_c}{c_0}\right)\right] \cdot \exp\left[-j\pi k_r \beta(\beta - 1) t_r^2\right] \mathrm{src}(f_a, \beta t_r; r_0). \quad (27)$$

The RVP correction factor is expressed as

$$H_{\mathrm{RVPC}}(f_a, f_r) = \exp\left(-j\frac{\pi f_r^2}{k_r \beta}\right). \quad (28)$$

Step 8 (inverse frequency scaling transform). Multiply $Ss_{\mathrm{RVPC}}(f_a, t_r; r_0)$ with the inverse frequency scaling factor $H_{\mathrm{IFS}}(f_a, t_r)$ which is

$$H_{\mathrm{IFS}}(f_a, t_r) = \exp\left[j\pi k_r \beta(\beta - 1) t_r^2\right]. \quad (29)$$

Step 9. Secondary range compression: multiply the signal with the secondary range compression factor $H_{\mathrm{SRC}}(f_a, t_r; r_c)$ which is described as

$$H_{\mathrm{SRC}}(f_a, t_r; r_c) = \mathrm{src}(f_a, \beta t_r; r_c)^*, \quad (30)$$

where the approximation $r_c \approx r_0$ is required.

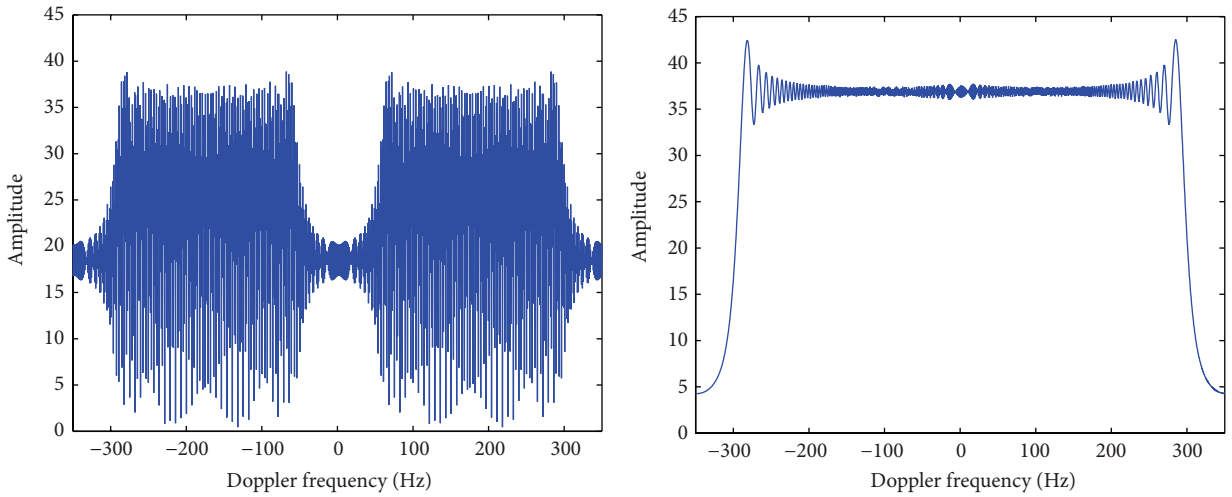

Figure 4: The azimuth aliasing spectrum before reconstruction filters (a) and the aliasing-removal spectrum after reconstruction filters (b).

Step 10. Bulk range shift: multiply the signal with the bulk range shift factor $H_{\mathrm{BV}}(f_a, t_r; r_c)$ which is described as

$$H_{\mathrm{BV}}(f_a, t_r; r_c) = \exp\left[j\frac{4\pi k_r r_c}{c_0}\left(\frac{1}{\beta} - 1\right)\left(\beta t_r - \frac{2r_c}{c_0}\right)\right]. \tag{31}$$

In actual implementation, Step 8 to Step 10 can also be completed at the same time. We obtain

$$\begin{aligned} Ss_{\mathrm{RCMC}}(f_a, t_r; r_0) &= Ss_{\mathrm{RVPC}}(f_a, t_r; r_0) \cdot H_{\mathrm{IFS}} \cdot H_{\mathrm{SRC}} \cdot H_{\mathrm{BV}} \\ &\approx \exp\left(-j\frac{4\pi r_0 \beta}{\lambda}\right) \\ &\quad \times \exp\left[-j\frac{4\pi k_r (r_0 - r_c)}{c_0 \beta}\left(\beta t_r - \frac{2r_c}{c_0}\right)\right]. \end{aligned} \tag{32}$$

Step 11. Apply FFT to $Ss_{\mathrm{RCMC}}(f_a, t_r; r_0)$ in range dimension. At this time, the range compression is completed as follows:

$$\begin{aligned} &Ss_{\mathrm{RCMC}}(f_a, f_r; r_0) \\ &= \frac{T}{\beta}\exp\left\{-j\frac{4\pi f_r r_c}{\beta c_0}\right\}\exp\left(-j\frac{4\pi r_0 \beta}{\lambda}\right) \\ &\quad \cdot \mathrm{sinc}\left[\pi\frac{T}{\beta}\left(f_r + \frac{2k_r (r_0 - r_c)}{c_0}\right)\right]. \end{aligned} \tag{33}$$

Step 12. The 2D focused image of DBF FMCW SAR is obtained after azimuth matched filtering [18].

4. Simulation Results

The parameters of an example FMCW SAR system using dual channels combined with DBF are listed in Table 1. The corresponding parameters of single channel FMCW SAR, which is very similar to MicroBSAR described in [6], are also given. There are two parts in the simulation. One is imaging simulation, the other is performance simulation.

4.1. System Parameters Design. To achieve the required resolution in azimuth, the Doppler bandwidth must be greater than 700 Hz. The transmit antenna length in azimuth should be less than 0.2 m. According to the swath width, the transmit antenna length in elevation can be chosen to be 2.9 cm, which corresponds to 40° beamwidth. The transmit antenna gain is 19.5 dB with the antenna efficiency 0.5.

The receive antenna is the same with the transmit antenna for single channel FMCW SAR. In the two-channel system, the receive antennas are placed in azimuth. The receive antenna gain is still the same. However the overall receive antenna length in azimuth reaches 0.4 m.

According to the Nyquist theorem, the PRF of classic FMCW SAR should be greater than the Doppler bandwidth. However, the PRF of DBF FMCW SAR can be chosen to be 700/2 Hz using two receive channels. To ensure a slant range resolution of 0.1 m, a chirp bandwidth of 1.5 GHz is necessary. The range processing gain 66.3 dB is obtained for DBF FMCW SAR. Nevertheless, that value of single channel FMCW SAR is only 63.3 dB. The sampling frequency of DBF FMCW SAR and single channel system are 16 MHz and 32 MHz, respectively. All the parameters are listed in Table 1.

4.2. Imaging Simulation. The target raw data are simulated using the two-channel system parameters listed in Table 1 by (9). To investigate the method of DBF technology and the effects of the continuous antenna motion, the raw data are processed by using the algorithm described in Figure 3.

The azimuth reconstruction is shown in Figure 4. Figure 4(a) shows the azimuth aliasing spectrum of the first channel signal in the two-channel system before reconstruction filter. After filters of $P_1(f_a)$ and $P_2(f_a)$, respectively, add the first channel signal and the second

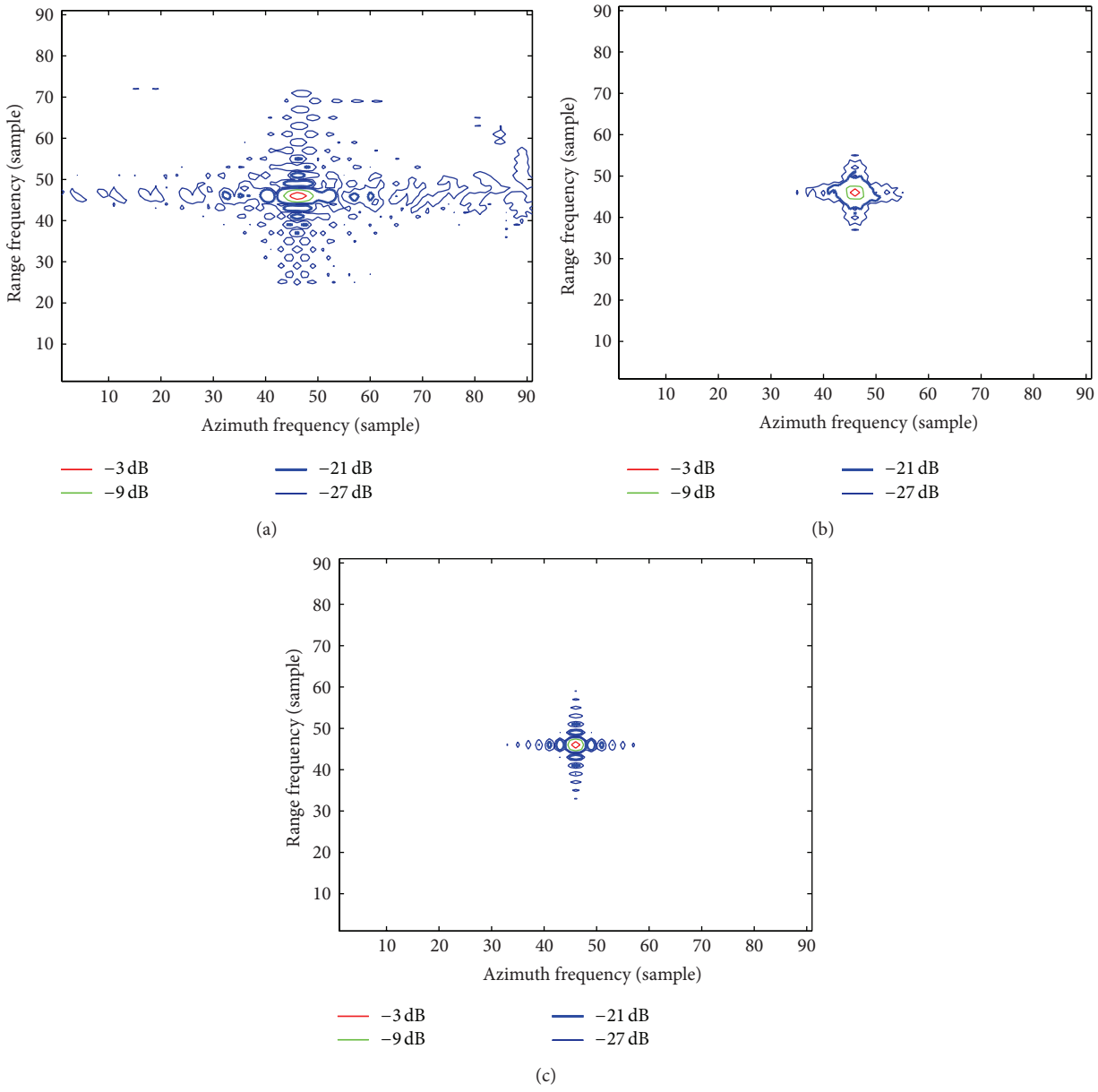

FIGURE 5: Contour plots of impulse response function of a point target without azimuth reconstruction (a), without Doppler frequency correction (b), and with azimuth reconstruction and Doppler frequency correction (c).

channel signal together. Then the azimuth spectrum is completely reconstructed. The reconstruction result is shown in Figure 4(b). The DBF coherently combines the two channel signals in azimuth and reconstructs a wide Doppler spectrum about 700 Hz.

Using the parameters of the two-channel example system, the signal processing presented in Section 3.3 is simulated. Figure 5 plots the 2D contour maps of the impulse response function of a point target. Only the values above −27 dB are plotted. The result of the proposed processing algorithm is plotted at the bottom. Figure 5(a) is the result without azimuth reconstruction. The performance is seriously degraded because the azimuth spectrum is overlapped as Figure 4(a) shows. To explore the characteristic of FMCW SAR distinguished with pulse SAR, Figure 5(b) illustrates the result without Doppler frequency correction factor which is expressed as (24). In terms of the resolution and shape of the response, it is shown that the reconstruction is successful and the impact of the motion within one sweep in FMCW SAR needs to be compensated.

4.3. Performance Simulation. Using the parameters in Table 1, NESZ for DBF FMCW SAR has been calculated over a range of incidence angles, which is shown in Figure 6. The result for single channel system is also shown in Figure 6. When calculating NESZ, the receiver noise figure is chosen

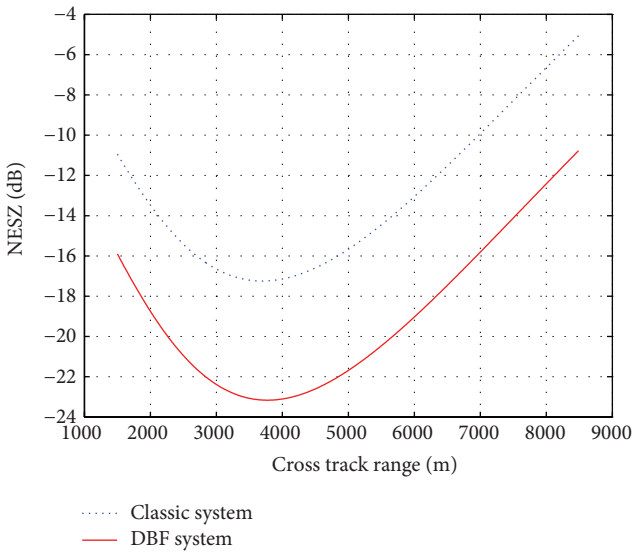

Figure 6: NESZ versus cross track range for DBF (solid) and single channel FMCW SAR (dotted).

as 3 dB. The DBF FMCW SAR achieves a NESZ below −10 dB along the entire swath. 5 W of transmitted power is sufficient to image vegetation and farmland. However, the result of classic FMCW SAR in the edge of the swath is only −5 dB, which is not sufficient to obtain good far-range imagery. The reason is that there is higher signal gain for DBF FMCW SAR.

5. Conclusions

A multichannel receive antenna FMCW SAR system combined with DBF is introduced. DBF FMCW SAR overcomes the limitation of high PRF caused by high azimuth resolution. It has higher receive antenna gain and range processing gain than single channel system. The received signal of DBF FMCW SAR is modeled. The impact of continuous antenna motion which is the main characteristic of FMCW SAR is negligible in multichannel azimuth reconstruction for DBF FMCW SAR, but it must be considered in the process during RCM correction. The whole signal processing diagram is given. Simulated point target experiments have been performed to verify the processing diagram successfully. Future works will include performance analysis thoroughly, moving target indication, and the miniaturization of the system.

Conflict of Interests

The authors declare that there is no conflict of interests regarding the publication of this paper.

Acknowledgment

This work was supported by the National Natural Science Foundation of China (nos. 41301397).

References

[1] E. Zaugg, D. Long, M. Edwards et al., "Using the MicroASAR on the NASA SIERRA UAS in the Characterization of Arctic Sea Ice Experiment," in *Proceedings of the IEEE International Radar Conference (RADAR '10)*, pp. 271–276, Washington, DC, USA, May 2010.

[2] M. Edrich, "Ultra-lightweight synthetic aperture radar based on a 35 GHz FMCW sensor concept and online raw data transmission," *IEE Proceedings: Radar, Sonar and Navigation*, vol. 153, no. 2, pp. 129–134, 2006.

[3] M. Weiss, O. Peters, and J. Ender, "A three dimensional SAR system on an UAV," in *Proceedings of the IEEE International Geoscience and Remote Sensing Symposium (IGARSS '07)*, pp. 5315–5318, Barcelona, Spain, July 2007.

[4] E. Zaugg, M. Edwards, D. Long, and C. Stringham, "Developments in compact high-performance synthetic aperture radar systems for use on small unmanned aircraft," in *Proceedings of the IEEE Aerospace Conference (AERO '11)*, pp. 1–14, Big Sky, Mont, USA, March 2011.

[5] A. Meta, J. J. M. de Wit, and P. Hoogeboom, "Development of a high resolution airborne millimeter wave FM-CW SAR," in *Proceedings of the 1st European Radar Conference (EuRAD '04)*, pp. 209–212, Amsterdam, The Netherlands, October 2004.

[6] M. C. Edwards, *Design of a continuous-wave synthetic aperture radar system with analog dechirp [M.S. thesis]*, Brigham Young University, Provo, Utah, USA, 2009.

[7] B. R. Jean and J. W. Rouse Jr., "A multiple beam synthetic aperture radar design concept for geoscience applications," *IEEE Transactions on Geoscience and Remote Sensing*, vol. 21, no. 2, pp. 201–207, 1983.

[8] A. Currie and M. A. Brown, "Wide-swath SAR," *IEE Proceedings F: Radar and Signal Processing*, vol. 139, no. 2, pp. 122–135, 1992.

[9] G. D. Callaghan and I. D. Longstaff, "Wide-swath space-borne SAR using a quad-element array," *IEEE Proceedings: Radar, Sonar and Navigation*, vol. 146, no. 3, pp. 159–165, 1999.

[10] M. Suess, B. Grafmueller, and R. Zahn, "A novel high resolution, wide swath SAR system," in *Proceedings of the International Geoscience and Remote Sensing Symposium (IGARRS '01)*, pp. 1013–1015, Sydney, Australia, July 2001.

[11] W. van Rossum, M. Otten, and P. van Dorp, "Multichannel FMCW SAR," in *Proceedings of the 9th European Conference on Synthetic Aperture Radar (EUSAR '12)*, pp. 279–282, Nuremberg, Germany, April 2012.

[12] A. Meta, E. Imbembo, C. Trampuz, A. Coccia, and G. de Luca, "A selection of MetaSensing airborne campaigns at L-, X- and ku band," in *Proceedings of the IEEE International Geoscience and Remote Sensing Symposium (IGARSS '12)*, pp. 4571–4574, Munich, Germany, July 2012.

[13] M. C. Edwards and E. C. Zaugg, "Design of a compact, modular, multi-frequency band, multi-mode, multi-channel synthetic aperture radar," in *Proceedings of the 9th European Conference on Synthetic Aperture Radar (EUSAR '12)*, pp. 44–47, Nuremberg, Germany, April 2012.

[14] X. Qin, W. Zhan, Z.-H. Jiang, and H.-F. Kan, "Improving FMCW SAR system performance by digital beamforming," in *Proceedings of the IEEE International Geoscience and Remote Sensing Symposium (IGARSS '12)*, pp. 4557–4560, Munich, Germany, July 2012.

[15] N. Gebert, G. Krieger, and M. A. Moreira, "Digital beamforming on receive: techniques and optimization strategies for high-resolution wide-swath SAR imaging," *IEEE Transactions on*

Aerospace and Electronic Systems, vol. 45, no. 2, pp. 564–592, 2009.

[16] Z.-H. Jiang and K. Huang-Fu, "Squint LFMCW SAR data processing using doppler-centroid-dependent frequency scaling algorithm," *IEEE Transactions on Geoscience and Remote Sensing*, vol. 46, no. 11, pp. 3535–3543, 2008.

[17] J. C. Curlander and R. N. McDonough, *Synthetic Aperture Radar: Systems and Signal Processing*, John Wiley & Sons, New York, NY, USA, 1991.

[18] J. Mittermayer, A. Moreira, and O. Loffeld, "Spotlight SAR data processing using the frequency scaling algorithm," *IEEE Transactions on Geoscience and Remote Sensing*, vol. 37, no. 5, pp. 2198–2214, 1999.

[19] E. C. Zaugg and D. G. Long, "Theory and application of motion compensation for LFM-CW SAR," *IEEE Transactions on Geoscience and Remote Sensing*, vol. 46, no. 10, pp. 2990–2998, 2008.

[20] A. Meta, P. Hoogeboom, and L. P. Ligthart, "Signal processing for FMCW SAR," *IEEE Transactions on Geoscience and Remote Sensing*, vol. 45, no. 11, pp. 3519–3532, 2007.